energy&fuels

pubs.acs.org/EF
Article

Pyrolysis of Polyethylene: Chemical Kinetics, Mass Transfer, and Reflux System

Published as part of Energy & Fuels special issue "Recent Advances in Thermochemical Recycling of Plastics".

Dwiputra M. Zairin, M. Pilar Ruiz, and Sascha R. A. Kersten*

Cite This: https://doi.org/10.1021/acs.energyfuels.4c05204

ABSTRACT: First, this paper investigates the interplay between reaction kinetics and mass transfer rates in the pyrolysis of polyethylene (PE) in the temperature range of 420 to 480 °C. Experimental results confirmed that the bond-breaking rate is high, shown by the reduction in average molecular weight of the reacting PE from 186 to 3.5 kDa in 2 min at 450 °C. The evaporation rate differs with reactor type and sets the mass loss rate and the molecular weight distribution of the condensed product. At 450 °C, first-order mass loss rate constants of 5×10^{-2} and 3×10^{-3} s^{-1} were observed in a screen-heater reactor and a semibatch reactor, respectively, while the average molecular weights of the condensed product were 2.3 and 0.6 kDa (mass-average MW by gel permeation chromatography), respectively. A mathematical model, involving bond-breaking and evaporation, was able to describe the experimentally observed fast initial cracking followed by evaporation. Second, the effect of adding a reflux system to the semibatch reactor was experimentally studied, showing that tested reflux temperatures (300−350 °C) set the molecular weight distribution of the condensed product, independently of the investigated reactor temperature. Notably, at a reactor temperature of 450 °C and reflux temperature of 350 °C, the average molecular weight by gas chromatography/mass spectrometry of the condensed product was found to be 164 Da. The study concludes that while refluxing improves the quality of the condensed product by reducing its average molecular weight, it also leads to a reduction in the liquid production rate and an increase in the permanent gas yield.

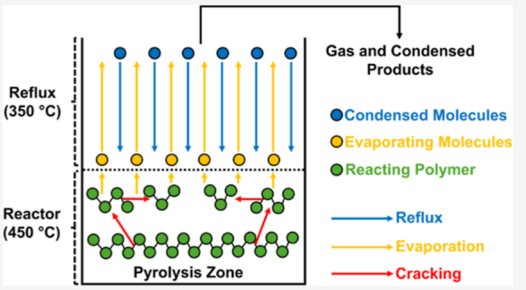

1. INTRODUCTION

Pyrolysis has emerged as a technology with the potential to play a role in the chemical recycling of plastic waste.[1−5] The first part of this paper focuses on further understanding[6] the interplay between the bond-breaking and evaporation rates, and their impact on reactor design and product distribution.[6] Evaporation is used here to denote all phenomena by which molecules can leave the reaction zone. Obviously, the evaporation rate is the mass loss rate of pyrolysis. Polyethylene is used as a model component in this study. Previous studies using unconventional reactors, such as the screen-heater reactor and pulse-heated reactor have demonstrated that the intrinsic bond-breaking rates of plastic pyrolysis are high.[6−8] For instance, in a recent paper, we reported high mass loss rates for the pyrolysis of polyethylene in a screen-heater reactor, designed to limit heat and mass transfer resistances.[6] First-order mass loss rate constants of 1 and 5×10^{-2} s^{-1} were found for 500 and 450 °C, respectively. This revelation uncovered a discrepancy between the intrinsic reaction rate of plastic pyrolysis and the mass loss rate, which is often lower and attributed to mass transfer limitations. This paper aims to demonstrate that the intrinsic reaction rate is high and remains consistent across reactor types while the mass loss rate varies. A mathematical model was developed and compared to the experimental results.

Better control of product distribution is important to enhance the commercial viability of pyrolysis. For instance, one of the current focuses in the field of pyrolysis is on the production of light naphtha oil (hydrocarbon with 5−12 carbon atoms) from plastic waste.[9−13] This naphtha fraction will serve as a (co)feedstock in an existing naphtha steam cracker unit to produce monomers. However, challenges persist in obtaining naphtha-dominated oil due to broad product distribution and wax formation. In a previous study, we reported that conducting polyethylene pyrolysis at a lower temperature (420 °C) resulted in a lighter condensed product, compared to at a higher temperature (500 °C).[6] This counterintuitive phenomenon highlights the role of evaporation, where higher temperatures increase the evaporation

Received: October 24, 2024
Revised: December 6, 2024
Accepted: December 10, 2024

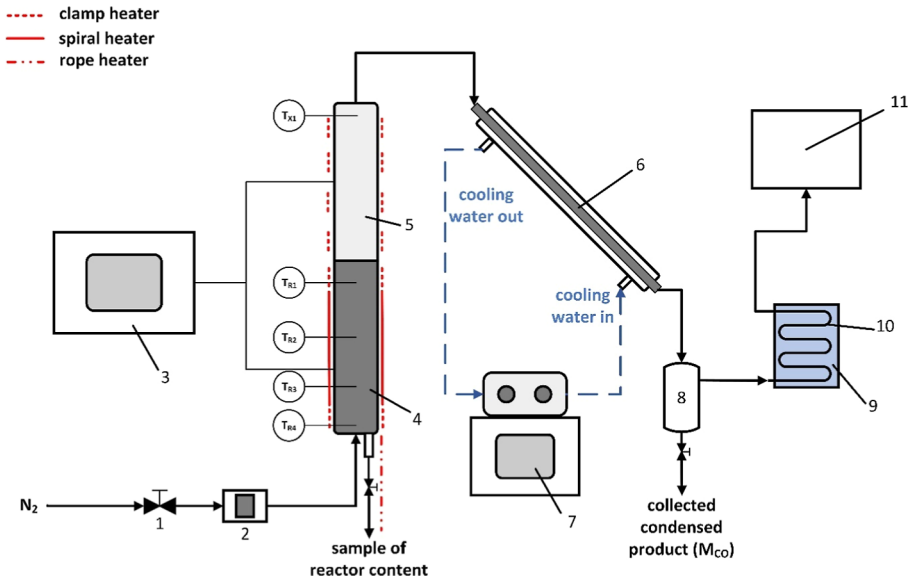

Figure 1. Schematic representation of the pyrolysis setup. (1) Valve; (2) nitrogen flow meter; (3) PID controller; (4) reactor unit; (5) reflux unit; (6) condenser; (7) water bath; (8) collection vessel; (9) ice bath; (10) coil condenser; (11) gas bag. T_{R1}, T_{R2}, T_{R3}, and T_{R4} are thermocouples inside the reactor unit. T_{X1} is a thermocouple inside the reflux unit.

rate, leading to rapid evaporation of cracked molecules from the reacting molten phase, preventing them from further cracking. While a lighter product distribution is desirable, lowering the pyrolysis temperature also decreases the reaction rate. Consequently, to achieve the same productivity as at higher temperatures, a larger reactor size would be necessary.

To optimize the product distribution while maintaining high reaction kinetics, pyrolysis reactors with reflux are proposed. This principle comprises setting the top section of the reactor to have a lower temperature than the main part.[14−20] By doing so, the heavier fractions of the pyrolysis gas can be condensed and subsequently flow back into the reactor to undergo further cracking. Hassibi et al. found that a reflux temperature of 125 °C in pyrolysis of polypropylene at 480 °C increased the composition of C_7−C_{10} to 87.2 wt % as compared to 45 wt % without reflux where heavier compounds (C_{17}+) predominated.[18] Dobó et al. conducted a similar study on reflux using mixed plastics, operating at a reactor temperature of 700 °C and varying reflux temperatures from 150 to 300 °C.[19] Their findings showed that the composition of the obtained oil was significantly influenced by the changes in reflux temperature, where lowering the reflux temperature resulted in lighter products.

While their work highlighted the potential of using a reflux system to control product distribution, it primarily focused on varying the reflux temperature. The effect of changing the reactor temperature while maintaining constant reflux temperature has not been discussed. Recently, Deka and Misra conducted a study on the pyrolysis of polyethylene in a reflux-assisted autoclave reactor across a range of reactor temperatures from 350 to 500 °C with water at 5−10 °C as cooling medium in the reflux condenser.[21] Their findings showed that increasing the reactor temperature from 415 to 500 °C while keeping the same cooling medium temperature in reflux resulted in a significant increase in gas yield and a corresponding suppression of liquid yield. Despite these findings, the effect of changing the reactor temperature on product composition was not addressed.

Reactor temperature is a critical factor in determining the reaction kinetics and consequently, product distribution. Therefore, in this study, we will investigate the impact of reactor temperature on product yield, production rate, and product composition while keeping a constant reflux temperature. We hypothesize that the molecular weight (distribution) of the condensed product is determined by the reflux temperature, leaving the temperature of the reactor zone to fix the production rate. This hypothesis will be tested in the second part of this paper, where also the advantages and drawbacks of using reflux will be discussed.

2. MATERIALS AND METHODS

2.1. Materials. Low-density polyethylene (LDPE) was obtained from Sabic in the form of pellets with an average diameter size of 3−5 mm. The average molecular weight of the LDPE is 186 kDa with a polydispersity of 9.2. Additionally, LDPE with a lower average molecular weight of 4 kDa (polydispersity of 2.3) was obtained from Sigma-Aldrich in powder form, with particle sizes smaller than 600 μm.

Nonporous α-alumina spheres with a diameter of 3 mm were used as the packing material in the reflux zone. These alumina spheres were supplied by Baan Machines BV with a purity of more than 92 wt % with the largest impurities being SiO_2 with a composition of 3.8 wt %. To remove the possibility of a catalytic effect of alumina in the reflux zone, another experiment was performed using 3 mm glass spheres (Carl Roth A557.1). We concluded that the change in the materials of the packing was not affecting the results of the experiment significantly. More information about this is available in the Supporting Information S.1.

2.2. Pyrolysis Setup. *2.2.1. Semibatch Reactor.* The pyrolysis experiments were carried out in a semibatch reactor unit, as depicted in Figure 1. The reactor unit comprised a stainless-steel reactor with dimensions of 56 cm in length and 3 cm in internal diameter. Heat was supplied to the reactor via a spiral heater along its outer wall, with additional clamp heaters at the top and bottom ensuring uniform heating. The temperatures inside the reactor were measured using thermocouples placed at four different sections as shown in Figure 1. A direct connection at the top of the reactor was established with an additional stainless-steel tube, which serves as the reflux unit, measuring 56 cm in length and 5 cm in internal diameter. Clamp

https://doi.org/10.1021/acs.energyfuels.4c05204
Energy Fuels XXXX, XXX, XXX−XXX

heaters were positioned at four different locations to heat the reflux unit uniformly.

Alumina spheres with a diameter of 3 mm were used as packing material to enhance condensation in the reflux. To assess the vapor−liquid equilibrium conditions inside the reflux unit, we conducted experiments with alumina spheres of different sizes: 2 cm, 6 mm, and 3 mm. The results showed that hardly any changes were observed in product yield and composition upon further decreasing the size from 6 to 3 mm, suggesting that vapor−liquid equilibrium was already achieved in the reflux unit under the given operating conditions. More information about this is available in the Supporting Information S.2. For experiments without reflux, packing materials were not used and the temperature of the reflux zone was set to the same temperature as the reactor.

At the start of the experiment, 90 to 360 g of LDPE were put inside the reactor at room temperature. Then, the entire setup was purged by using nitrogen gas to ensure the removal of oxygen. The flow of nitrogen sweep gas was 18 N mL/min during reactions (200 N mL/min during purging). After confirming that there was no leakage in the entire setup, heat was introduced to both the reactor and reflux unit. This reactor employed a ramping heating program, which enabled the sample inside the reactor to heat up at a heating rate of approximately 12 °C/min to reach the set point temperature. Once the set point was reached, the reactor temperature was maintained constant for the remainder of the experiment. An example of the temperature profile in this setup is available in Supporting Information S.3.

As the temperature of pyrolysis was reached, vapors began to form within the reactor and subsequently entered the reflux unit. Vapors that did not condense in the reflux unit were directed through a collection system, initially passing through a condenser set at 10 °C. This temperature can be adjusted to 70−80 °C in case of wax deposition and potential clogging. The resulting oil and wax products were collected in a collection vessel, which could be opened at any desired time interval for product collection and analysis. The remaining gas effluent then passed through a coil condenser, cooled at 0−5 °C using an ice bath, to condense the remaining oil and wax fraction. Lastly, the remaining noncondensed gas was collected in a gas bag for analysis. The time of the reaction started ($t = 0$) upon achieving the desired temperature within the reactor. The pyrolysis experiment was then allowed to proceed for 6 h. Additionally, a connection was installed at the bottom of the reactor to enable the collection of reactor contents during the reaction. This section is heated to 250 °C, a temperature low enough to quench the reactions and high enough to maintain flow properties. The experiments were performed in duplicate to assess repeatability, and the calculated 95% confidence interval of the yields was below 1.6 wt % from all the process conditions.

The equations used for calculating the product yield are presented as follows, where Y_R, Y_{CPCS}, Y_{CPP}, and Y_{TCP} are the yield of residue in reactor, yield of condensed product in collection system, yield of condensed product in packing materials (alumina spheres), and yield of total condensed product, respectively.

$$Y_R = \frac{m_R}{m_{Feedstock}} \times 100\% \tag{1}$$

$$Y_{CPCS} = \frac{m_{CV} + m_C + m_{CO}(end)}{m_{Feedstock}} \times 100\% \tag{2}$$

$$Y_{CPP} = \frac{m_P}{m_{Feedstock}} \times 100\% \tag{3}$$

$$Y_{TCP}(t) = \frac{m_{CO}(t) + \frac{m_{CV} + m_C + m_P}{t_f} \times t}{m_{Feedstock}} \times 100\% \tag{4}$$

In these equations, m_R represents the mass of the remaining residue within the reactor at the end of the experiment. The condensed product, which can be oil, wax, or a mixture of both, is primarily recovered in the collection system comprising the condenser and collection vessel. However, some amount of condensed product remains in the packing materials at the end of the experiment. m_{CV}, m_C, and m_P are masses of condensed product remaining in the collection vessel, condenser, and packing materials (alumina spheres), respectively. m_P was determined by measuring the mass difference of the packing materials before and after the experiment. Initially, the packing materials were clean and dry, but after the experiment, they contained condensed products on their surface. Similarly, m_{CV}, and m_C were determined by measuring the differences in the mass of the collection vessel and condenser before (when they were empty) and after the experiment, containing condensed products.

m_{CO} is the mass of collected condensed products flowing out of the collection vessel and can be measured over time while m_{CV}, m_C, and m_P can only be measured at the end of the experiment. To construct total condensed product yield versus time graphs, m_{CV}, m_C, and m_P values are distributed evenly into m_{CO} over time as shown in eq 4, where t_f represents the total duration of the experiment, and t is the time at which the measurement is made, or the elapsed time during the experiment. To calculate the gas product yield (Y_{Gas}), the following equations were used.

$$m_{Gas} = \sum_i \left(\frac{P_{ambient} \frac{y_i}{y_{N_2}} V_{N_2} MW_i}{RT_{ambient}} \right) \tag{5}$$

$$Y_{Gas} = \frac{m_{Gas}}{m_{Feedstock}} \times 100\% \tag{6}$$

where m_{Gas} is the total mass of all gas components, $P_{ambient}$ is 1 bar, y_i is the volume fraction of component i, and y_{N_2} is the volume fraction of nitrogen. These volume fractions are measured by gas chromatography. Additionally, V_{N_2} is the volume of nitrogen which was obtained by the volumetric flow multiplied by the experiment time. MW_i is the molecular weight of component i, R is the universal gas constant, and $T_{ambient}$ is 25 °C.

The total yield (mass balance closure) from the experiment (Y_{Total}) can be calculated by the following equation.

$$Y_{Total} = Y_R + Y_{CPCS} + Y_{CPP} + Y_{Gas} \tag{7}$$

Additionally, the yield of the final gas and condensed products can also be defined by the carbon number of each component using the following equation.

$$Y_{Carbon,i} = \frac{m_{Carbon,i}}{m_{Feedstock}} \times 100\% \tag{8}$$

where $m_{Carbon,i}$ represents the mass of gas and condensed products classified by their carbon number, determined through gas chromatography (GC) and gas chromatography/mass spectrometry (GC−MS) analysis, respectively.

Since it is not possible to directly measure the amount of plastic remaining inside the reactor during the pyrolysis experiment, the remaining plastic is estimated based on the total yield of gas and condensed products over time. This estimated value is then used to calculate the mass loss rate of the reaction. The calculation is expressed by the following equation.

$$w_r(t) = 1 - \frac{Y_{TCP}(t) + \frac{Y_{Gas}}{t_f} \times t}{Y_{Total}} \tag{9}$$

where w_r is the mass fraction remaining in the reactor at a certain time.

2.2.2. Screen-Heater Reactor. The main features of the screen-heater reactor are summarized as follows. The reactor consists of a glass vessel, within which a plastic sample was pressed between two metal mesh screens (approximate thickness of ∼45 μm) to ensure uniform heating across the sample. The screens, along with the plastic sample, were rapidly heated to the desired reaction temperature with a heating rate of ∼5000 °C/s. The screens were maintained at the desired temperature for a specific duration, depending on the required reaction time. The glass vessel was placed inside a liquid nitrogen bath

https://doi.org/10.1021/acs.energyfuels.4c05204
Energy Fuels XXXX, XXX, XXX−XXX

(∼−180 °C), which serves to quench and condense the cracked molecules as they evaporate and leave the screens under vacuum conditions. This quenching prevents further degradation and facilitates the collection of condensed products on the wall of the glass vessel. This reactor configuration minimizes the mass and heat transfer limitations, allowing for more accurate measurement of the intrinsic chemical kinetics of the pyrolysis process. A detailed explanation of the reactor is available in our earlier works.[22−24]

2.3. Analysis of Pyrolysis Products. *2.3.1. Gas Chromatography (GC).* The composition of the gas product was determined using a Varian 450-RGA gas chromatography (GC) system. The system was equipped with three different channels for analysis. Channel 1 utilized a Molsieve 5A column (Agilent CP1306) and a Hayesep Q column (Agilent CP1305) to determine hydrogen composition. Channel 2 consisted of a Molsieve 13X column (Varian CP1309), a Hayesep N column (Varian CP1307), and a Hayesep Q column (Varian CP1308) to detect CO, CO_2, and O_2. The last channel comprised a CP-Sil 5CB column (Varian CP1310) and a Select Al_2O_3/MAPD column (Varian CP7433) to detect different hydrocarbon components ranging from C_1 to C_5, as well as traces of higher hydrocarbons lumped together as C_6+.

2.3.2. Gel Permeation Chromatography (GPC). The molecular weight distribution of the resulting condensed products was measured using a gel permeation chromatography (GPC) Agilent 1260 Infinity series equipped with a refractive index detector (RID) and UV detector operating at 254 nm. A 3 GPC PLgel 3m MIXED-E column was employed with pure tetrahydrofuran (THF) as the mobile phase. Polystyrene solutions with molecular weights ranging from 162 to 27810 Da were used as calibration. The oil and wax samples were dissolved in THF (1 wt %). Unless stated otherwise, all mass-averaged molecular weight values in this paper were measured using GPC. This analysis provides the RID response as a function of elution volume, which correlates with the molecular weight distribution of the samples. In this paper, we present the RID response on the *y*-axis as an arbitrary unit (au), normalized by dividing each response value by the maximum response value.

2.3.3. Gas Chromatography−Mass Spectrometry/Flame Ionization Detector (GC−MS/FID). The composition of the resulting condensed products was analyzed using the GC 7890A MS 5975C system from Agilent Technologies, equipped with an autosampler and a flame ionization detector (FID). The GC column utilized was an Agilent HP-5MS (HP19091S-433). During the analysis, the column temperature was initially set at 45 °C and maintained for 10 min. Subsequently, the temperature was increased at a rate of 3 °C per minute until it reached 280 °C. The oil and wax samples were dissolved in *n*-heptane (5 wt %) to quantify the hydrocarbons of C_8−C_{33}. Meanwhile, to quantify the hydrocarbons of C_7 and lower, the oil and wax samples were dissolved in *n*-undecane (5 wt %). Hydrocarbons of C_{33}+ were calculated by the difference. The quantification was calibrated using a standard of known hydrocarbon compounds with various carbon ranges, namely *n*-hexane, *n*-heptane, *n*-undecane, *n*-dodecane, *n*-tetradecane, *n*-pentadecane, *n*-hexadecane, *n*-eicosane, and *n*-dotriacontane, which represents every lumped group used in this study.

2.3.4. Viscosity and Density. An Ubbelohde viscometer, calibrated by Paragon Scientific Limited per ASTM D 446, was used to measure the kinematic viscosity of the pyrolysis oil at a temperature of 25 °C. At the same temperature, the density of the oil was measured by pycnometer Blaubrand 10 mL, DIN ISO 3507. The dynamic viscosity is then calculated by the following equation.

$$\text{Dynamic viscosity} = \text{kinematic viscosity} \times \text{density} \tag{10}$$

2.4. Modeling. Polymer pyrolysis involves complex mechanisms with numerous reaction pathways, including bond cracking, radical recombination, and hydrogen shift, making accurate modeling challenging.[25] In this study, we developed a model to describe the pyrolysis of polyethylene that specifically focuses on cracking (the cleavage of larger hydrocarbons into smaller ones) and the escape of reaction products from the reacting polymers. Escaping from the reactive zone is possible via evaporation, sublimation, and ejection of aerosols. Only evaporation is considered for now. The main objective of this model is to explore how these processes influence the molecular weight distribution of reacting polymer, product, and mass loss rates during pyrolysis. The model equations include mole balances for the liquid and gas phases, as well as equations for the cracking and evaporation rates. The parameters for the model were fitted to the experimental data obtained from semibatch reactor experiments. The details of the model are discussed below.

The reacting polymer is modeled as a linear chain of $(CH_2)_i$ units. For each polymer of i unit (N_i), a mole balance is solved for both reacting plastic (N_i^L) and evaporating pyrolysis gas (N_i^G)

$$\frac{dN_i^L}{dt} = -E_i + F_i - K_i \tag{11}$$

$$\frac{dN_i^G}{dt} = E_i \tag{12}$$

$$\frac{dm}{dt} = -\sum_{i=1}^{i\_max} MW_i E_i \tag{13}$$

m represents the mass of plastic in the semibatch reactor. N_i^L denotes the number of moles of each component i in the liquid phase, from which the molecular weight distribution of the reactor content is calculated. Similarly, N_i^G is used to determine the molecular weight distribution of the evaporated products. The cracking rate (K_i) refers to the rate at which N_i undergoes cracking reactions, resulting in the breakdown of larger hydrocarbons into smaller ones. In pyrolysis experiments, the resulting products comprise both saturated and unsaturated hydrocarbons. However, at this stage, this is not considered, as the primary focus is to assess how cracking and evaporation rates affect the carbon number distribution of the products.

The cracking process in this model includes the cleavage of bonds connecting each monomeric carbon unit, allowing each unit to crack in $(i - 1)$ distinct ways. Furthermore, it is assumed that all possible cracking pathways have equal probability, meaning that the rate constant, k_c, is consistent for all cracking reactions. This approach is commonly implemented in modeling cracking processes,[25,26] though the specific assumptions may vary. The cracking rate for each hydrocarbon is described by the following equation.

$$N_i \rightarrow N_j + N_{i-j} \text{ for } (i > j) \wedge (i > 1) \wedge (j > 0) \tag{14}$$

$$K_i = (i - 1)k_c N_i^L \tag{15}$$

N_i is also formed by cracking reactions. The formation rate (F_i) represents the rate at which N_i is formed through cracking reactions of larger hydrocarbons N_j where $j > i$.

$$F_i = 2\sum_{j=i+1}^{i\_max} k_c N_j^L \tag{16}$$

We formulated the evaporation rate (E_i) based on Raoult's law and a mass transfer coefficient that is a function of the molecular weight, capturing the behavior of volatile components in mixtures and avoiding a first-order assumption, which we will validate in this study from experimental results. The evaporation rate is defined by the following equations.

$$E_i = A_e k_{e,0} D_i \left(\frac{P_i^*}{RT_{reactor}} x_i^L\right) \text{ for } i \le 100 \tag{17}$$

$$x_i^L = \frac{N_i^L}{\sum_{i=1}^{i\_max} N_i^L} \tag{18}$$

$$D_i = \frac{1}{\left(\frac{MW_i}{MW_{CH_2}}\right)^a} \tag{19}$$

https://doi.org/10.1021/acs.energyfuels.4c05204
Energy Fuels XXXX, XXX, XXX−XXX

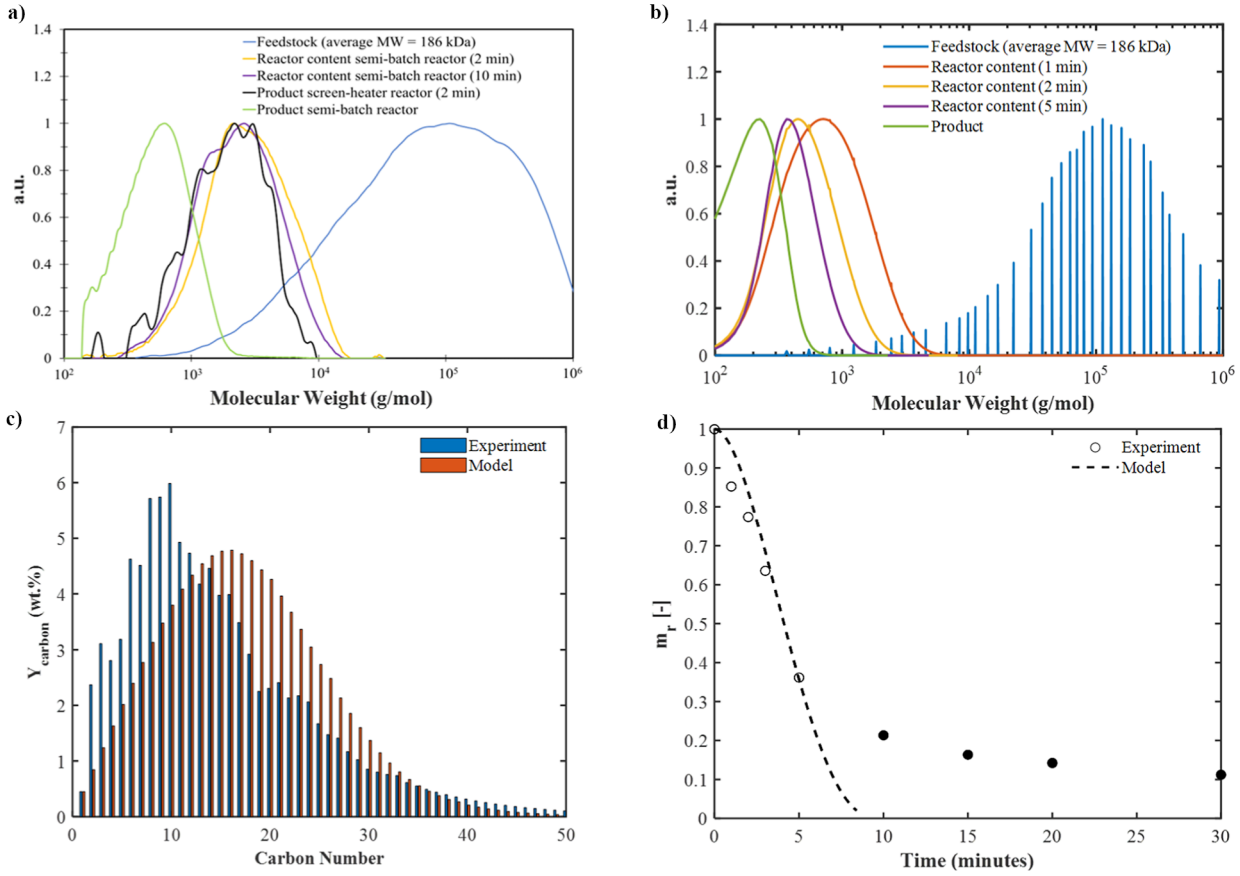

Figure 2. Comparison of experimental and modeling results (180 g of 186 kDa LDPE at 450 °C). (a) Reactor content MWD at different times, experimental; (b) reactor content MWD at different times, modeling results; (c) carbon yield comparison of the final product between normalized experiment and model (semibatch reactor); (d) total condensed product yield comparison between normalized experiment and model (semibatch reactor).

$$\log(P_i^*) = A_i - \frac{B_i}{T_{\text{reactor}} + C_i} \tag{20}$$

Therefore, E_i represents a zeroth order process if x_i^L is constant. The vapor pressure is obtained using the Antoine equation, assuming that only polymer units $i \leq 100$ can evaporate from the reacting liquid phase. The parameters for the Antoine equation were obtained from literature and the NIST Webbook.[27] However, due to the limited availability of data for hydrocarbons larger than C_{20}, these parameters were calculated through extrapolation.[27]

The initial values are based on the actual LDPE used in the experiments, with an average molecular weight of 186 kDa. For simplification, instead of assigning a mole fraction to each CH_2 unit, the mole fraction is allocated to only 40 different lumped fractions. These lumped fractions reflect the real molecular weight distribution of the LDPE used (see Figure 2b).

The model contains three unknown parameters, viz. k_c, $A_e k_{e,0}$ and a. k_c and $k_{e,0}$ are functions of temperature which can be described with the Arrhenius equation, thereby adding two parameters. In this paper, we did not parametrize the equations fully because this requires better validation of the underlying assumptions and more experimental data than available at the time of writing. We focus in this account on the trends predicted by the model, and the comparison of those with experimental observations. Only for the base case experiment (180 g of feed of LDPE 186 kDa) at 450 °C the Matlab (2021b version) routine fmincon was used to parametrize the model, which provided a first estimate of k_c, $A_e k_{e,0}$, and a at that temperature. The numerical integration of these equations was performed with the built-in ode45 solver. The parameter fitting process was based on the difference between the experimental and modeled carbon yield distribution of the final product, as well as the mass loss rate. Given that the mass balance closure of the experiment was not 100% (see Figure 6), the experimental values for carbon yield were first normalized using the following equation.

$$Y_{\text{Carbonnorm},i} = \frac{Y_{\text{Carbon},i}}{\sum_{i=1}^{q} Y_{\text{Carbon},i}} \times 100\% \tag{21}$$

The objective function for fitting the parameters is defined in the following equation.

$$f_j = \frac{1}{q}\sum_{i=1}^{q}\left(\frac{Y_{\text{Carbon norm},i} - Y_{\text{Carbon model},i}}{Y_{\text{Carbon norm},i}}\right)^2 + \frac{1}{p}\sum_{j=1}^{p}\left(\frac{w_{r,j} - w_{\text{r model},j}}{w_{r,j}}\right)^2 \tag{22}$$

3. RESULTS AND DISCUSSION

3.1. Kinetics: Bond-Breaking, Evaporation, and Mass Loss Rates. Experiments of pyrolysis of LDPE were conducted in the semibatch reactor at 450 °C without reflux. After 2 and 10 min of reaction, the plastic sample from inside the reactor was collected and the molecular weight distribution was measured. Figure 2a shows that the bond-breaking rate in polyethylene pyrolysis is high. In a short period of time, the average molecular weight of the reacting plastic (the reactor content) decreased from 186 to ~3.5 kDa. This reduction is comparable to the molecular weight distribution of products obtained from our screen heater reactor at the same

https://doi.org/10.1021/acs.energyfuels.4c05204
Energy Fuels XXXX, XXX, XXX−XXX

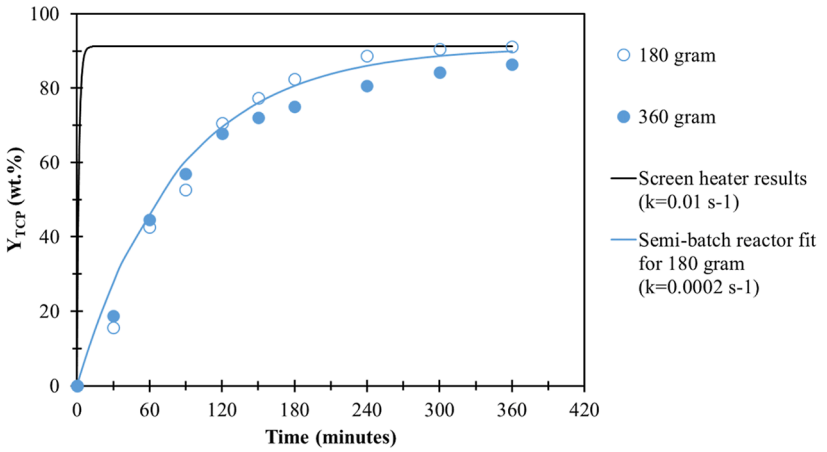

Figure 3. Total condensed product yield versus time from pyrolysis of LDPE 186 kDa in the semibatch reactor at 420 °C with two different initial masses of feedstock, 180 and 360 g.

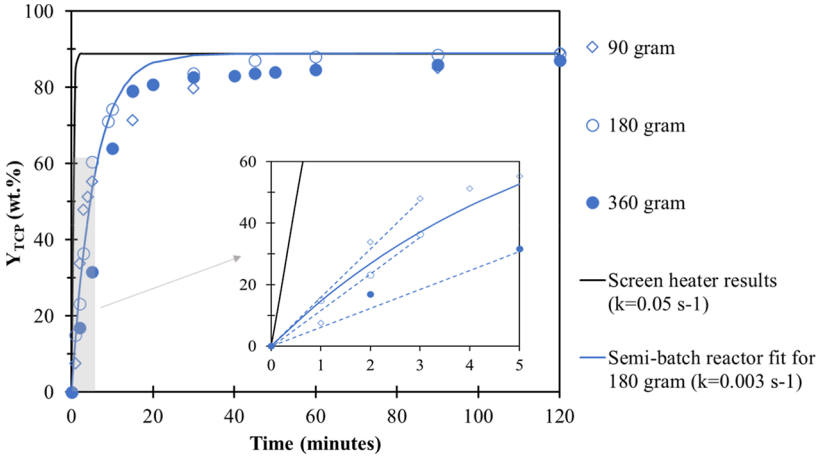

Figure 4. Total condensed product yield versus time from pyrolysis of LDPE 186 kDa in the semibatch reactor at 450 °C with different initial masses of feedstock, 90, 180, and 360 g.

temperature, which has minimal heat and mass transfer limitations.[6,22−24,26] This shows that the intrinsic bond-breaking rate of polyethylene pyrolysis is fast, independent of the reactor type. The difference lies between the evaporation rates of different reactors, affecting the mass loss rate and final molecular weight distribution of the condensed product. In the screen-heater reactor, where evaporation is fast, cracked polyethylene fragments evaporate immediately upon reaching an average molecular weight of 2.3 kDa. In contrast, in the semibatch reactor with a lower evaporation rate, polyethylene must undergo further cracking to reach a significant evaporation rate, resulting in a condensed product with an average molecular weight of 600 Da (Figure 2a).

For reactor temperature of 450 °C and 180 g feed, the model was parametrized, resulting in $k_c = 3.3 \times 10^{-4}$ s^{-1}, $A_e k_{e,0} = 2.2 \times 10^{-5}$ m_{gas}^3/s, and $a = 1 \times 10^{-2}$. Hence, due to the low value of a, D_i can be set to 1. With these parameters, the model was able to capture the trend observed in the experimental results presented in Figure 2a. However, the model failed to predict the molecular weight distribution of the reactor content quantitatively, where the predicted value obtained by the model was significantly lower than the experimental results (compare Figure 2a,b). On the other hand, the model was able to reasonably describe the molecular weight distribution (MWD) of the pyrolysis product and the initial mass loss rate observed in the experiment (Figure 2c,d). However, a discrepancy arises in the mass loss rate at the first minute and after 10 min, when approximately 80% of the mass has already been lost. During the first minute, the experimental data shows a faster rate, possibly due to some extent of pyrolysis occurring before the reactor reaches 450 °C. After 10 min, the model predicts a faster rate. Since the experimental mass loss is estimated based on the collection of condensed products, this difference is likely attributed to the nature of condensed product collection in the experiment. After 10 min, the reactor is nearly empty, and the condensed product exits slowly and in small quantities. This leads to a slower apparent mass loss rate from the experimental data after 10 min (shown by the filled black markers in Figure 2d).

In future work, we plan to improve the model parametrization and validation using a larger data set that includes different reactor temperatures, initial amount of feedstock, and different molecular weights of the feedstock. Additionally, we aim to enhance the reaction mechanism by incorporating a more detailed reaction mechanism based on radicals,[25] which will enable the model to predict the composition of both saturated and unsaturated hydrocarbons in the product. This larger data set will help in refining the regression parameters, thereby improving the accuracy of the model predictions and discussing its use for reactor design applications. Here, we

https://doi.org/10.1021/acs.energyfuels.4c05204
Energy Fuels XXXX, XXX, XXX−XXX

conclude that the modeling approach shows promise but requires further validation to fully demonstrate its applicability.

Figures 3 and 4 depict the condensed product yield over time in the semibatch reactor, at two different temperatures, 420 and 450 °C, respectively, and with different initial amounts of feedstock. First-order mass loss rate constants were calculated by the following equation.

$$k = -\frac{1}{t}\ln\left(1 - \frac{Y_{TCP}(t)}{Y_{TCP}(\text{end})}\right) \quad (23)$$

where k is the first-order mass loss rate constant, in s^{-1}, and $Y_{TCP}(\text{end})$ is the yield of the total condensed product at the end of the experiment.

In a recent paper, we reported high mass loss rates for the pyrolysis of polyethylene in a screen-heater reactor designed to limit heat and mass transfer resistances.[6] First-order mass loss rate constants of 1 and 5×10^{-2} s^{-1} were found for 500 and 450 °C, respectively (see Figure 4). The observed mass loss rates are not first order. However, initially, we have chosen to determine and present first-order rate constants to enable mutual comparison of data sets, later, we discuss deviation from first-order behavior. In the semibatch reactor, at 450 °C, pyrolysis of PE took ca. 20 min (time to reach ca. 90% conversion, see Figure 4) which corresponds to a first-order mass loss rate constant of ca. 3×10^{-3} s^{-1}, being ca. 16 times lower than the one determined in the screen-heater reactor.

At 420 °C, the total condensed product yield versus time trajectory is not affected by the amount of feedstock used as shown in Figure 3, indicating a first-order reaction behavior. This suggests that at 420 °C, the bond-breaking rate is low and becomes the limiting factor for the mass loss rate. The first-order mass loss rate constant is 2×10^{-4} s^{-1}.

Conversely, as shown in the inset graph of Figure 4, at 450 °C, the total condensed product yield is affected by the amount of feed used; the higher the amount of feedstock, the slower the initial production of the condensed product, indicating a change in mass loss order to below one, because of the semizero order evaporation rate (see eq 17).

Additionally, we analyzed the effect of the initial molecular weight of the feedstock, by comparing the pyrolysis of LDPE of 4 and 186 kDa at 450 °C. Figure 5 shows the results of total condensed product yield with time for the two feedstocks, where it is evident that the production rate in both cases is quite similar, and thus not affected by the initial molecular weight of the polymer. This is expected, as it was experimentally found that the LDPE of 186 kDa cracked down to an average molecular weight of 3.5 kDa within 2 min (Figure 2a). The molecular weight distribution of the condensed products in both cases is also similar as shown in Supporting Information S.4.

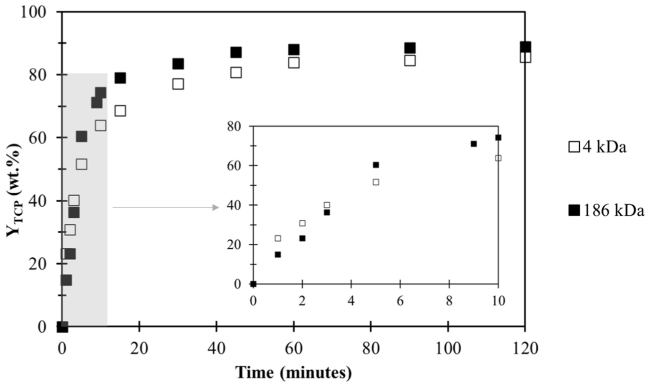

Figure 5. Total condensed product yield versus time from pyrolysis of LDPE in the semibatch reactor at 450 °C with a variation of the initial molecular weight of the feedstock (initial mass of feedstock = 180 g).

3.2. Pyrolysis with Reflux. The reactor temperature was systematically varied between 420, 450, and 480 °C while keeping the temperature of the reflux constant at 350 °C. Figure 6 shows the product yield of the corresponding

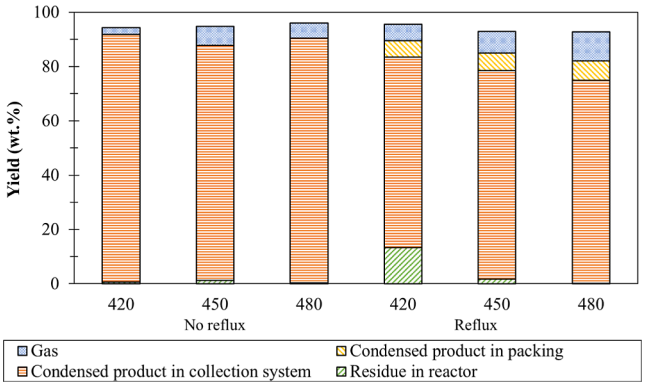

Figure 6. Product yield of pyrolysis of LDPE at different reactor temperatures with and without reflux (feedstock = 180 g of LDPE 186 kDa; reflux temperature = 350 °C; reaction time = 6 h).

experiments, where the mass balance closure remains high for every condition, surpassing 90 wt %. It can be observed from the graph that for the experiments without reflux, the changes in reactor temperature did not result in significant changes in the yield of the condensed product after 6 h of reaction. Gas production is higher at 450 and 480 °C. Conversely, when employing reflux, elevating the reactor temperature led to a notable decrease in solid residue in the reactor (14.1 and 0.1 wt % for 420 and 480 °C, respectively). We concluded that the major part of the residue within the reactor at the end of the experiment was neither char nor unconverted plastic, but the condensed substance remaining from continuously evaporating to the reflux zone and condensing back to the reactor zone, i.e., continuously refluxing under those conditions. The amount of residue at 420 °C indicates that at this temperature, the cracking rate is not sufficient to break down the condensed molecules redirected from the reflux zone and most of it will immediately evaporate again. Further details supporting this conclusion are provided in the Supporting Information S.5.

To get more information regarding the production rate of the condensed product, the total condensed product yield over time at different process conditions, as well as the first-order mass loss rate (eq 23), are depicted in Figure 7. Once again, the first-order mass loss rate was selected only for consistent comparison to estimate the kinetics across different conditions. Clearly, the use of reflux lowered the rate of condensed product collection, indicated by a first-order mass loss rate that is five times lower than without reflux at a reactor temperature of 450 °C. A similar trend is observed at different reactor temperatures (see Figure 7). From a process design perspective, the production rate obtained from the experiments with reflux could be a drawback. To achieve the same capacity as without reflux, a reactor with reflux would need to be substantially larger. This could be counter-acted by increasing

https://doi.org/10.1021/acs.energyfuels.4c05204
Energy Fuels XXXX, XXX, XXX−XXX

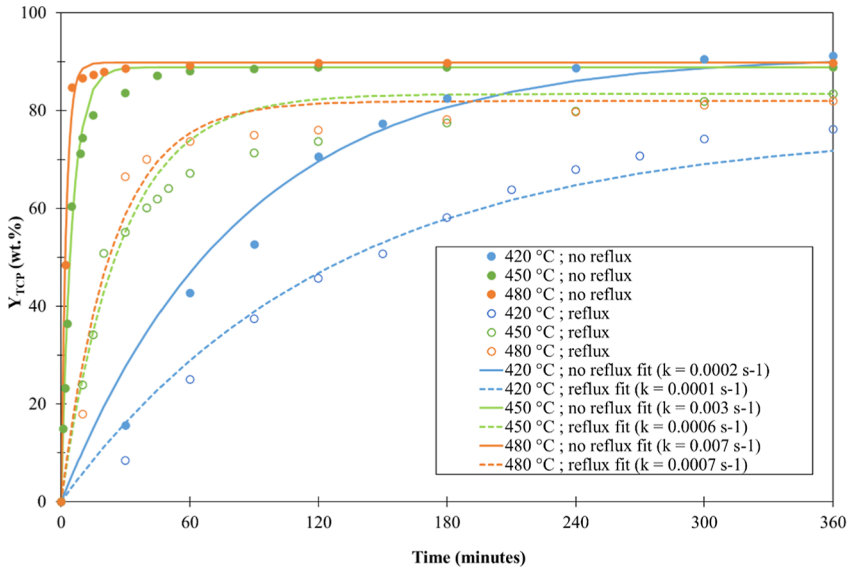

Figure 7. Total condensed product yield versus time of pyrolysis of LDPE at different reactor temperatures with and without reflux (feedstock = 180 g of LDPE 186 kDa; reflux temperature = 350 °C; reaction time = 6 h).

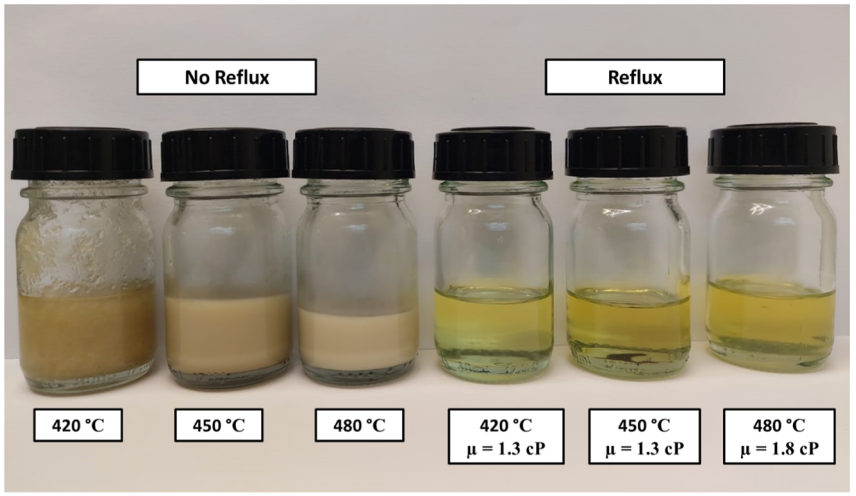

Figure 8. Physical appearance of collected condensed products at different reactor temperatures with and without reflux (feedstock = 180 g of LDPE 186 kDa; reflux temperature = 350 °C; reaction time = 6 h).

the temperature of the reaction zone. However, it has been observed that this only applies to the lower reactor temperature range. As shown in Figure 7, increasing the reactor temperature to approximately 450 °C with reflux could be more than enough to achieve the same rate as the reactor temperature of 420 °C without reflux. In contrast, raising the reactor temperature to 480 °C with reflux does not suffice to match the rate at 450 °C without reflux. In all cases, refluxing will result in a higher energy demand for the reactor because re-evaporation of the condensed fraction is needed. The extracted energy from the condenser (reflux system) can be used to preheat the feed.

In terms of the produced permanent gases, elevating the reactor temperature leads to an increase in total gas production and changes in the gas composition (see Figure 6). At a reactor temperature of 480 °C, there was an increase in both ethylene and propylene production, while the propane production was suppressed as compared to a lower temperature (Supporting Information S.6). Additionally, the use of reflux increases the production of permanent gases at all the reactor temperatures. The product yield reported in Figure 6 indicates that reflux has a larger effect on permanent gas production compared to increasing the reactor temperature. Although these permanent gases are valuable resources for heating and chemical production, they could pose a disadvantage if the desired production is the naphtha fraction.

The physical appearance of the collected condensed products from different reactor temperatures is depicted in Figure 8. In the absence of reflux, the condensed product at 450 and 480 °C predominantly consists of wax, indicating a higher molecular weight compared to 420 °C, which is a mixture of oil and wax. Conversely, with the use of reflux, all reactor temperatures resulted in a free-flowing oil with similar values of viscosity (1.3−1.8 cP). This already shows that the usage of a reflux system leads to lower average molecular weight.

The composition of the condensed products in the collection system was characterized by GC−MS analysis. These products include various compound groups, such as *n*-alkanes, 1-alkenes, and isoalkanes, which were grouped based

https://doi.org/10.1021/acs.energyfuels.4c05204
Energy Fuels XXXX, XXX, XXX−XXX

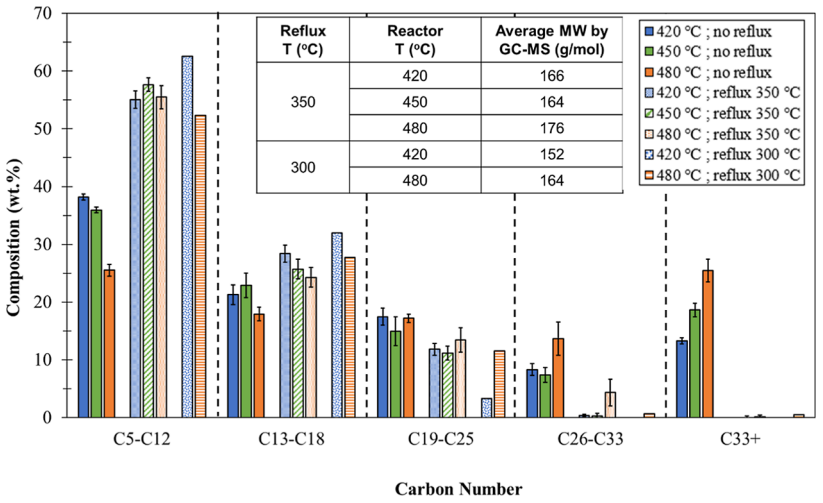

Figure 9. Composition of collected condensed product at different reactor temperatures with and without reflux (feedstock = 180 g of LDPE 186 kDa; reflux temperature = 350 °C; reaction time = 6 h).

on their carbon number. The carbon numbers were further lumped into several fractions as shown in Figure 9. As anticipated, without reflux, notable differences were observed in each fraction from different reactor temperatures. High amounts of C_{33}+ fraction were produced, constituting 13.3, 18.6, and 25.5 wt % respectively for reactor temperatures of 420, 450, and 480 °C. Consequently, the naphtha fractions (C_5−C_{12}) were relatively low, with the highest obtained at 420 °C at 38.2 wt %. In contrast, employing a reflux at 350 °C yielded better results: independent of the reactor temperature, the naphtha fraction was ca. 55 wt % and the C_{33}+ fraction was below 1 wt % with average MW by GC−MS of 164 Da, indicating that reflux temperature is the main factor in controlling the amount of heavies in the product distribution. To validate these findings, an additional set of experiments was conducted at a reflux temperature of 300 °C. Also at this temperature, hardly any heavies (C_{33}+) were present in the product when using the reflux system. More information is available in Supporting Information S.7.

Overall, it is concluded that refluxing enables the production of a lighter oil, at the expense of a slightly lower oil yield (higher gas yield), increased energy consumption (due to re-evaporation of the refluxed liquid), and longer reaction time.

4. CONCLUSIONS

This study investigated the pyrolysis of LDPE using semibatch and screen heater reactors. It was found that the intrinsic bond-breaking rate in polyethylene pyrolysis is rapid, evidenced by a significant reduction in molecular weight from 186 kDa to approximately 3.5 kDa within 2 min at 450 °C, irrespective of reactor type. The evaporation rate, however, differs between the reactor types.

Initial modeling efforts have resulted in a reasonable prediction of the molecular weight distribution of the product and initial mass loss rate.

Introducing a reflux temperature of 350 °C at a reactor temperature of 450 °C enhanced the production of lower hydrocarbon fraction and narrowed the molecular weight distribution of the products (average MW by GC−MS = 164 Da). The properties of the oil product with reflux were consistent across the different reactor temperatures of 420, 450, and 480 °C, indicating that the reflux temperature is the primary factor in controlling the product quality, independent of the reactor temperature. However, using reflux results in a lower liquid production rate and an increase in permanent gas yield, necessitating a trade-off between oil quality, production rate, and oil yield.

■ ASSOCIATED CONTENT

Data Availability Statement

Data will be made available on request.

Supporting Information

The Supporting Information is available free of charge at https://pubs.acs.org/doi/10.1021/acs.energyfuels.4c05204.

Supporting information S.1 to S.7 (PDF)

■ AUTHOR INFORMATION

Corresponding Author

Sascha R. A. Kersten − *Sustainable Process Technology, Faculty of Science and Technology, University of Twente, Enschede 7522 NB, The Netherlands;* orcid.org/0000-0001-8333-2649; Email: s.r.a.kersten@utwente.nl

Authors

Dwiputra M. Zairin − *Sustainable Process Technology, Faculty of Science and Technology, University of Twente, Enschede 7522 NB, The Netherlands*

M. Pilar Ruiz − *Sustainable Process Technology, Faculty of Science and Technology, University of Twente, Enschede 7522 NB, The Netherlands; Circular Chemical Engineering, Maastricht University, Geleen 6167 RD, The Netherlands;* orcid.org/0000-0003-1437-5578

Complete contact information is available at: https://pubs.acs.org/10.1021/acs.energyfuels.4c05204

Notes

The authors declare no competing financial interest.

■ ACKNOWLEDGMENTS

The authors gratefully acknowledge the Institute for Sustainable Process Technology (ISPT) of The Netherlands and The Dutch Polymer Institute (DPI) within the framework of the INREP project (MOOI plan, 2020, An Integrated

https://doi.org/10.1021/acs.energyfuels.4c05204
Energy Fuels XXXX, XXX, XXX−XXX

Approach towards Recycling of Plastics) and partners. The authors would also like to thank several additional partners involved in this work: Benno Knaken, Ronald Borst, Raymond Spanjer, and Erna Fränzel-Luiten from the University of Twente for their technical support., Demcon Suster, B.V. for making the pyrolysis setup available, Riccardo Casasanta for his assistance in the experimental work, and Wouter Schiphorst and Robbin Vriesema for their assistance in sample preparation for analytical techniques.

NOMENCLATURE

a	dimensionless parameter [-] in eq 19,
A_e	area of evaporation [m_e^2]
A_i	Antoine equation constant A for unit i [-]
B_i	Antoine equation constant B for unit i [-]
C_i	Antoine equation constant C for unit i [-]
D_i	dimensionless parameter to describe the internal diffusion of unit i within the reacting plastic [-]
E_i	evaporation rate of unit i from the reacting plastic to gas phase [mol/s]
F_i	the formation rate of unit i from the cracking of larger unit j [mol/s]
k	first-order mass loss rate constant [s^{-1}]
k_c	bond cracking rate constant [s^{-1}]
$k_{e,0}$	evaporation rate constant [$m_{gas}^3/(m_e^2\ s)$]
K_i	cracking rate of unit i [mol/s]
m	mass of reacting plastic in the reactor [g]
m_C	mass of the remaining condensed product in the condenser at the end of experiment [g]
m_{Carbon}	mass of the product based on the carbon number [g]
m_{CO}	mass of the condensed product flowing out of the collection vessel over time [g]
m_{CV}	mass of the remaining condensed product in the collection vessel at the end of experiment [g]
$m_{Feedstock}$	mass of the feedstock used in the experiment [g]
m_{Gas}	the total mass of gas produced from the experiment [g]
m_P	mass of the remaining condensed product in packing materials at the end of experiment [g]
m_R	mass of the remaining residue in the reactor at the end of experiment [g]
MWD	molecular weight distribution
MW_i	the molecular weight of unit i [g/mol]
N_i	moles of unit i [mol]
p	number of data points of mass fraction remaining in reactor [-]
$P_{ambient}$	the ambient pressure [Pa]
P_i^*	vapor pressure of pure component i [Pa]
q	number of data points of carbon yield of the final product [-]
R	universal gas constant [(m^3 Pa)/(K mol)]
t	time at which the measurement is taken (s)
$T_{ambient}$	the ambient temperature [K]
t_f	total duration of the experiment [s]
$T_{Reactor}$	temperature of the reactor [K]
V_{N_2}	the volume of nitrogen used during the experiment [m^3]
w_r	mass fraction remaining in the reactor at a certain time from experimental data [-]
$w_{r\ model}$	mass fraction remaining in the reactor at a certain time calculated by model [-]
x_i	mole fraction of component i in the liquid phase [-]
Y_{carbon}	experimentally obtained yield of the product based on the carbon number[-]
$Y_{carbon\ model}$	yield of the product based on the carbon number calculated by the model [-]
$Y_{carbon\ norm}$	the normalized value of the experimentally obtained yield of the product based on the carbon number[-]
Y_{CPCS}	yield of condensed product in collection system [-]
Y_{CPP}	yield of condensed product in packing materials [-]
Y_{Gas}	yield of the gas product [-]
y_i	the volume fraction of component i in the gas product [-]
y_{N_2}	the volume fraction of nitrogen in the gas product [-]
Y_R	yield of residue in reactor [-]
Y_{TCP}	yield of total condensed product [-]
Y_{Total}	total yield of the experiment [-]

SUPERSCRIPTS

G gas phase
L liquid phase (reacting plastic)

REFERENCES

(1) Chang, S. H. Plastic waste as pyrolysis feedstock for plastic oil production: A review. *Sci. Total Environ.* **2023**, *877*, 162719.
(2) Kartik, S.; Balsora, H. K.; Sharma, M.; Saptoro, A.; Jain, R. K.; Joshi, J. B.; Sharma, A. Valorization of plastic wastes for production of fuels and value-added chemicals through pyrolysis − A review. *Therm. Sci. Eng. Prog.* **2022**, *32*, 101316.
(3) Maqsood, T.; Dai, J.; Zhang, Y.; Guang, M.; Li, B. Pyrolysis of plastic species: A review of resources and products. *J. Anal. Appl. Pyrolysis* **2021**, *159*, 105295.
(4) Onwudili, J. A.; Insura, N.; Williams, P. T. Composition of products from the pyrolysis of polyethylene and polystyrene in a closed batch reactor: Effects of temperature and residence time. *J. Anal. Appl. Pyrolysis* **2009**, *86*, 293−303.
(5) Zhang, Y.; Chen, X.; Cheng, L.; Gu, J.; Xu, Y. Conversion of Polyethylene to High-Yield Fuel Oil at Low Temperatures and Atmospheric Initial Pressure. *Int. J. Environ. Res. Publ. Health* **2023**, *20*, 4048.
(6) Ruiz, M. P.; Zairin, D. M.; Kersten, S. R. A. On the intrinsic reaction rate of polyethylene pyrolysis and its interplay with mass transfer. *Chem. Eng. J.* **2023**, *469*, 143886.
(7) Mastalski, I.; Sidhu, N.; Zolghadr, A.; Maduskar, S.; Patel, B.; Uppili, S.; Go, T.; Wang, Z.; Neurock, M.; Dauenhauer, P. J. Intrinsic Millisecond Kinetics of Polyethylene Pyrolysis via Pulse-Heated Analysis of Solid Reactions. *Chem. Mater.* **2023**, *35*, 3628−3639.
(8) Sidhu, N.; Mastalski, I.; Zolghadr, A.; Patel, B.; Uppili, S.; Go, T.; Maduskar, S.; Wang, Z.; Neurock, M.; Dauenhauer, P. J. On the intrinsic reaction kinetics of polypropylene pyrolysis. *Matter* **2023**, *6*, 3413−3433.
(9) Kusenberg, M.; Eschenbacher, A.; Djokic, M. R.; Zayoud, A.; Ragaert, K.; De Meester, S.; Van Geem, K. M. Opportunities and challenges for the application of post-consumer plastic waste pyrolysis oils as steam cracker feedstocks: To decontaminate or not to decontaminate? *Waste Manage.* **2022**, *138*, 83−115.
(10) Kusenberg, M.; Zayoud, A.; Roosen, M.; Thi, H. D.; Abbas-Abadi, M. S.; Eschenbacher, A.; Kresovic, U.; De Meester, S.; Van Geem, K. M. A comprehensive experimental investigation of plastic waste pyrolysis oil quality and its dependence on the plastic waste composition. *Fuel Process. Technol.* **2022**, *227*, 107090.

https://doi.org/10.1021/acs.energyfuels.4c05204
Energy Fuels XXXX, XXX, XXX−XXX

(11) Kusenberg, M.; Roosen, M.; Zayoud, A.; Djokic, M. R.; Dao Thi, H.; De Meester, S.; Ragaert, K.; Kresovic, U.; Van Geem, K. M. Assessing the feasibility of chemical recycling via steam cracking of untreated plastic waste pyrolysis oils: Feedstock impurities, product yields and coke formation. *Waste Manage.* **2022**, *141*, 104−114.
(12) Lange, J. P. Managing Plastic Waste-Sorting, Recycling, Disposal, and Product Redesign. *ACS Sustain. Chem. Eng.* **2021**, *9*, 15722−15738.
(13) Donaj, P. J.; Kaminsky, W.; Buzeto, F.; Yang, W. Pyrolysis of polyolefins for increasing the yield of monomers' recovery. *Waste Manage.* **2012**, *32*, 840−846.
(14) Seth, D.; Sarkar, A. Thermal pyrolysis of polypropylene: Effect of reflux-condenser on the molecular weight distribution of products. *Chem. Eng. Sci.* **2004**, *59*, 2433−2445.
(15) Wajima, T.; Zar, Z. H.; Hideki, N. Oil production from polyethylene plastics by thermal pyrolysis using a reflux condenser. *Adv. Mater. Res.* **2014**, *1025−1026*, 842−845.
(16) Santos, E.; Rijo, B.; Lemos, F.; Lemos, M. A. N. D. A. A catalytic reactive distillation approach to high density polyethylene pyrolysis − Part 1 − Light olefin production. *Chem. Eng. J.* **2019**, *378*, 122077.
(17) Hassibi, N.; Vega-Bustos, Y. A.; Aissaoui, M. H.; Mauviel, G.; Burklé-Vitzthum, V. Thermochemical Recycling of Polystyrene by Pyrolysis: Importance of the Reflux to Maximize the Production of Styrene and BTEX. *Ind. Eng. Chem. Res.* **2023**, *62*, 13432−13439.
(18) Hassibi, N.; Quiring, Y.; Carré, V.; Aubriet, F.; Vernex-Loset, L.; Mauviel, G.; Burklé-Vitzthum, V. Analysis and control of products obtained from pyrolysis of polypropylene using a reflux semi-batch reactor and GC-MS/FID and FT-ICR MS. *J. Anal. Appl. Pyrolysis* **2023**, *169*, 105826.
(19) Dobó, Z.; Mahner, T.; Kecsmar, G.; Nagy, G. The Influence of Reflux Temperature on the Yield of Trasnportation Fuels during Plastic Waste Pyrolysis: The Influence of Reflux Temperature on the Yield. *Mater. Sci. Eng.* **2020**, *45*, 77−83.
(20) Suiuay, C.; Sudajan, S.; Katekaew, S.; Senawong, K.; Laloon, K. Production of gasoline-like-fuel and diesel-like-fuel from hard-resin of Yang (Dipterocarpus alatus) using a fast pyrolysis process. *Energy* **2019**, *187*, 115967.
(21) Deka, A.; Misra, R. D. Enhancement of fuel-grade oil yields from thermal pyrolysis of polyethylene and polystyrene through reflux condenser assisted autoclave reactor. *Clean Technol. Environ. Policy* **2024**, *26*, 2289−2308.
(22) Hoekstra, E.; van Swaaij, W. P. M.; Kersten, S. R. A.; Hogendoorn, K. J. A. Fast pyrolysis in a novel wire-mesh reactor: Design and initial results. *Chem. Eng. J.* **2012**, *191*, 45−58.
(23) Hoekstra, E.; Van Swaaij, W. P. M.; Kersten, S. R. A.; Hogendoorn, K. J. A. Fast pyrolysis in a novel wire-mesh reactor: Decomposition of pine wood and model compounds. *Chem. Eng. J.* **2012**, *187*, 172−184.
(24) Westerhof, R. J. M.; Oudenhoven, S. R. G.; Marathe, P. S.; Engelen, M.; Garcia-Perez, M.; Wang, Z.; Kersten, S. R. A. The interplay between chemistry and heat/mass transfer during the fast pyrolysis of cellulose. *React. Chem. Eng.* **2016**, *1*, 555−566.
(25) Levine, S. E.; Broadbelt, L. J. Detailed mechanistic modeling of high-density polyethylene pyrolysis: Low molecular weight product evolution. *Polym. Degrad. Stab.* **2009**, *94*, 810−822.
(26) Marathe, P. S.; Westerhof, R. J. M.; Kersten, S. R. A. Fast pyrolysis of lignins with different molecular weight: Experiments and modelling. *Appl. Energy* **2019**, *236*, 1125−1137.
(27) Kudchadker, A. P.; Zwolinski, B. J. Vapor Pressures and Boiling Points of Normal Alkanes, C21 to C100. *J. Chem. Eng. Data* **1966**, *11*, 253−255.

https://doi.org/10.1021/acs.energyfuels.4c05204
Energy Fuels XXXX, XXX, XXX−XXX